ARL-TR-8908 ● FEB 2020

DEVCOM ARMY RESEARCH LABORATORY

Preliminary Computational Analysis of Film Cooling on a Flat Plate at Different Blowing Ratios

by Waldo A Acosta, Douglas R Thurman, and Philip Poinsatte

NOTICES

Disclaimers

The findings in this report are not to be construed as an official Department of the Army position unless so designated by other authorized documents.

Citation of manufacturer's or trade names does not constitute an official endorsement or approval of the use thereof.

Destroy this report when it is no longer needed. Do not return it to the originator.

ARL-TR-8908 ● FEB 2020

Preliminary Computational Analysis of Film Cooling on a Flat Plate at Different Blowing Ratios

Waldo A Acosta and Douglas R Thurman
Vehicle Technology Directorate, CCDC Army Research Laboratory

Philip Poinsatte
Glenn Research Center, Cleveland, Ohio

REPORT DOCUMENTATION PAGE

Form Approved
OMB No. 0704-0188

1. REPORT DATE *(DD-MM-YYYY)*	2. REPORT TYPE	3. DATES COVERED (From - To)
February 2020	Technical Report	1 October 2018 – 30 September 2019

4. TITLE AND SUBTITLE
Preliminary Computational Analysis of Film Cooling on a Flat Plate at Different Blowing Ratios

5a. CONTRACT NUMBER

5b. GRANT NUMBER

5c. PROGRAM ELEMENT NUMBER

6. AUTHOR(S)
Waldo A Acosta, Douglas R Thurman, and Philip Poinsatte

5d. PROJECT NUMBER

5e. TASK NUMBER

5f. WORK UNIT NUMBER

7. PERFORMING ORGANIZATION NAME(S) AND ADDRESS(ES)
CCDC Army Research Laboratory
ATTN: FCDD-RLV-P
Cleveland, OH 44135

8. PERFORMING ORGANIZATION REPORT NUMBER
ARL-TR-8908

9. SPONSORING/MONITORING AGENCY NAME(S) AND ADDRESS(ES)

10. SPONSOR/MONITOR'S ACRONYM(S)

11. SPONSOR/MONITOR'S REPORT NUMBER(S)

12. DISTRIBUTION/AVAILABILITY STATEMENT
Approved for public release; distribution is unlimited.

13. SUPPLEMENTARY NOTES

14. ABSTRACT
A computational study of turbine film cooling on a flat plate was conducted. Advanced high-temperature ceramic-matrix-composite materials and manufacturing technologies offer the opportunity to discover new and improved film cooling technologies for gas-turbine engine airfoils that could significantly improve their performance. The computations were aimed at determining if commercially available computational fluid dynamics codes generate results with enough fidelity to choose between proposed concepts in a timely manner and limited user intervention. Since the accuracy of the results of the computations are directly tied to the mesh resolution, creating the mesh can be a time-consuming step and may require generating multiple meshes until finding the right one. The study used two commercial packages that feature automatic mesh generation capabilities, COMSOL Multiphysics and CONVERGE. The automated mesh generation utilizes the physics of the problem being studied to generate the most appropriate mesh. The computational results were compared with experimental data and showed that the meshes generated by both software packages were qualitatively and quantitatively in good agreement with the experimental data and provide substantive information to assess the potential of new proposed film cooling concepts in a timely manner, reducing experimental time and resources.

15. SUBJECT TERMS
film cooling, computational fluid dynamics, gas turbine engines, cooling effectiveness, heat transfer, blowing ratio

16. SECURITY CLASSIFICATION OF:			17. LIMITATION OF ABSTRACT	18. NUMBER OF PAGES	19a. NAME OF RESPONSIBLE PERSON
a. REPORT	b. ABSTRACT	c. THIS PAGE			Walter M Brennan
Unclassified	Unclassified	Unclassified	UU	25	19b. TELEPHONE NUMBER (Include area code) (410) 278-7601

Contents

List of Figures

Acknowledgments

Portions of this work were sponsored by the Advanced Air Transportation Technology Project within NASA's Advanced Air Vehicles Program. The authors acknowledge the help received by the COMSOL and CONVERGE customer support staff.

1. Introduction

Future improvements in gas-turbine engine thermodynamic efficiency will come from higher operating temperatures and pressures. To realize those benefits, the engines will need materials with improved temperature capabilities and/or improvements in cooling technology. This is more important in the high-pressure turbine (HPT) section, where the temperature of the hot exhaust gases from the combustor can exceed the melting temperature of the airfoil materials. Cooled ceramic-matrix-composite (CMC) materials are the prime enablers. CMCs have the potential to operate at material surface temperatures higher than the melting point of the alloys currently used in gas-turbine-engine turbine airfoils. The high-temperature capability in combination with the lower density of CMCs contribute to improvements to power density. Future gas-turbine engines will weigh less due to a combination of lower-density CMCs and corresponding weight reductions as a result of lower-weight turbine disks and reduced engine containment requirements due to reduced centrifugal forces. Boyle et al. showed that by applying proper design practices, CMCs can significantly improve HPT stage aerodynamic efficiency.[1]

A component of the proper design of an HPT is the film cooling holes, which are placed on turbine airfoils to distribute the cooling air evenly across the surface. The effectiveness of the cooling hole depends on the shape and the blowing ratio (BR). BR is defined as the ratio of the coolant flow rate $(\rho U)_c$ to the freestream flow rate $(\rho U)_\infty$. The shape, location, hole length-to-diameter (L/D) ratio, pitch-to-diameter ratio (P/D), and surface roughness of the cooling holes are some of the parameters that affect cooling effectiveness. In general, for cylindrical holes at compound angles and diffusion-type holes at low BRs (and low-density ratio), an increase in turbulence intensity leads to a deterioration of cooling effectiveness due to enhanced jet–freestream mixing in the near-hole region and increased losses. At high BRs, turbulence helps to provide cooling to the otherwise starved surface by mixing the lifted-off coolant jet with the surrounding hot gas. The aspect ratio (L/D) of the hole plays a role in the trajectory of the cooling jet and therefore should be taken in consideration when designing cooling holes. The proper P/D ensures the optimum amount of cooling in the regions between the cooling holes. For a more comprehensive review of parametric effects on film cooling holes see Bogard and Thole,[2] Bons et al.,[3] Shyam et al.,[4,5] and Sgarzi and Leboeuf.[6]

Improvements in computational fluid dynamics (CFD) codes and computing capacity have enabled better predictions of cooling hole performance and guide the design of more-efficient and more-durable HPTs. Many of those CFD codes are what are considered research codes, may not have a friendly graphical user interface

(GUI), and require a steep learning curve to properly use them. Since often the accuracy of the results depends on having the proper mesh or grid, the user may also need some knowledge in grid generation. The use of supercomputing clusters allows for highly fine meshes if needed, but availability may impact turnaround times to be useful in design in experiments cases when an optimal design might be the final objective. Commercial codes for the most part have a GUI that can guide the user to properly set up the simulation. However, many still require a mesh that is generated outside of the GUI.

Researchers at the NASA Glenn Research Center are conducting fundamental research on film cooling as it applies to future CMC airfoils. The research involves simulating the surface of a potential CMC design and experimentally evaluating the cooling performance of different film cooling hole configurations.

A simple flat-plate jet-in-crossflow model was experimentally evaluated to simulate the film cooling on a turbine blade. The scaled-up (12.5×) model included a flat and a "CMC-like" roughed surface and allowed multiple hole alignments to be studied. Navier–Stokes computations of the test model complement the experimental data and can be beneficial, guiding future testing.

The objective of this research was to investigate the potential of two commercial codes with automatic mesh-generation capabilities to meet the researchers' needs. The codes selected were CONVERGE and COMSOL Multiphysics. Both codes include a GUI, automatic mesh-generation capability, and conjugate heat transfer. For reasons discussed later, CONVERGE was used to conduct time-dependent, large eddy simulations (LESs) on a supercomputing cluster, and COMSOL Multiphysics was used for the steady-state calculations on a PC.

2. Experimental Setup and Conditions

2.1 Experimental Setup

Experiments were conducted in the small heat-transfer wind tunnel facility, SW-6, at the Glenn Research Center. Pictures of the experimental facility are shown in Fig. 1. The tunnel consists of an aluminum bellmouth, flow conditioning screens, and a square acrylic section 8.2 × 8.2 inches (0.21 × 0.21 m) square with 0.75-inch (0.02-m)-thick walls. The tunnel was connected to an electric fan downstream of the test section that pulled room air through. The film cooling jet test section pieces were attached to the floor of the tunnel. The test section floor piece used inserts with a varying number of holes and surface roughness, with acrylic (smooth or laser etched) and an acrylonitrile butadiene styrene (ABS) plate mounted to the outside bottom of the acrylic to provide an L/D of 2.

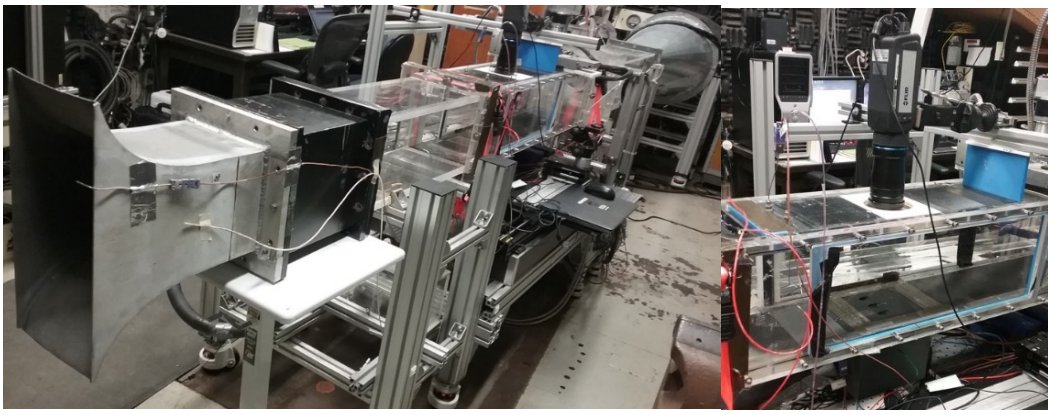

Fig. 1 (left) Glenn Research Center experimental facility; (right) experimental test section

Figure 2 shows the tunnel test section floor configuration. The thermal conductivity of the ABS thermoplastic is 0.17 W/(m·K), which is similar to acrylic with a nominal value of 0.18 W/(m·K). The coolant holes were inclined at 30° to the horizontal surface, and nominal hole diameter was 0.50 inches (0.0127 m). The hole spacing (P/D) used in this study was 3. An IR camera was used to measure surface temperature of the film cooling test section; the camera was mounted on top of the tunnel and the test section floor was viewed through a coated zinc selenide lens with an IR transmission of approximately 95%. Tunnel flow was at ambient conditions with a blade-realistic Reynolds number of 11,000 based on hole diameter and freestream velocity. Freestream velocity was 45 ft/s (13.7 m/s) at 75° F (297 K), and the turbulence intensity was measured to be nominally 1.5% at the inlet to the test section. In a normal film cooling situation, the coolant is at a lower temperature than the freestream temperature; however, the facility was limited in its ability to effectively heat the large volume of mainstream airflow. Thus, for this experiment the "coolant" was heated to provide the required temperature difference between the ambient flow and the plenum temperature. Previous work in this facility showed no significant difference in results between a cooled and a heated jet in crossflow for similar test conditions. The "coolant" flow was provided by blowing pressurized air through a flow meter and into a plenum attached to the underside of the test section floor plate. The "cooled" air was passed through a series of electrical heaters to provide plenum temperatures near 135° F (330 K).

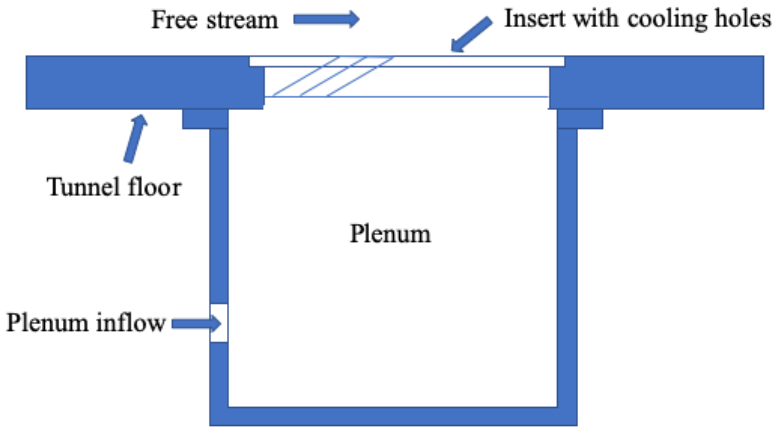

Fig. 2 Test section showing insert for cooling hole plate

A PC-based data-acquisition system was used to acquire data from pressure transducers and thermocouples. The tunnel flow rate was measured from a total pressure probe placed upstream of the test section and static pressure taps located on the sidewalls. Freestream temperature was measured with a thermocouple located upstream of the holes near the total pressure probe. "Coolant" conditions were measured with static pressure taps and thermocouples inside the plenum. IR measurements were acquired with a medium-resolution camera with 640- × 480-pixel IR camera, with images stored on a laptop computer. For a description of the IR measurement setup, see Shyam et al.[4]

2.2 Computational Setup

The computational domain extended 12 diameters upstream and 16 diameters downstream of the leading edge of the cooling holes. Spacing between the holes was equal to three-hole diameters. The computational domain of the plenum inlet extended 10 diameters upstream.

As previously stated, COMSOL Multiphysics was used to solve the Reynolds-averaged Navier–Stokes (RANS) equations. COMSOL Multiphysics is a general-purpose simulation software that uses finite element analysis and solver. The GUI guides the user through the process from defining the problem to plotting the results. COMSOL Multiphysics offers a variety of turbulence models to choose from. For this study we used the κ-ε and the shear stress transport (SST) models. The κ-ε model solves for κ, the turbulent kinetic energy, and ε (epsilon), the rate of turbulent kinetic energy dissipation. The model uses wall functions and has a good convergence rate and relatively low memory requirements. The SST model

combines the κ-ε model in the freestream and the κ-ω model near the walls. It was formulated to eliminate some of the weaknesses in the pure κ-ω and κ-ε models.

The meshes were generated using COMSOL's automated meshing capabilities, which take into consideration the physics of the problem being solved. For example, the software will insert a boundary layer mesh on the walls. The user has several mesh size choices, from extremely coarse to extremely fine. The finer the mesh, the larger the number of elements generated and memory needed. Due to memory limitations on the PC used in this study, a MacBook Pro with 16 GB of memory, the fine option was the smallest mesh size used. COMSOL also has an adaptive mesh refinement (AMR) option that lets the software improve the mesh to optimize the solution within the parameters specified. This feature was attempted in one particular case, but the software returned an error. According to customer support, when using AMR it is important to start with a good mesh; starting with a finer mesh than we had would have helped. Their recommendation was to perform a manual mesh-refinement study, which would, however, defeat our purpose of not having to generate the mesh manually.

Time-dependent simulations were performed using the CONVERGE commercial CFD code, which is a compressible Navier–Stokes solver based on a first-order predictor–corrector time-integration scheme and second-order finite-volume schemes for spatial discretization. It features a nonstaggered, collocated, computational grid framework using a Rhie–Chow interpolation technique to avoid spurious oscillations. An efficient geometric multigrid treatment is used to solve the pressure equation, and parallel computing is based on Message Passing Interface protocols. It provides the option of increasing resolution locally through static fixed-grid embedding and dynamically through AMR activated through user-specified criteria. The solver also provides a choice between a number of modeling options for the treatment of turbulence, including contemporary forms of the RANS and LES approaches. The computations were carried out using the dynamic structure LES model available in CONVERGE. It does not use turbulent viscosity to model the subgrid stress tensor; instead, it adds a transport equation for the subgrid kinetic energy.

The procedure for generating the structured mesh starts by defining a base mesh size, in this case 0.002 m. Then the user selects where and when to apply the AMR. AMR automatically refines the mesh based on fluctuating and moving conditions such as temperature or velocity. In this case AMR was applied to the velocity. The number of times the mesh is allowed to be refined is specified by the user and will be activated based on the subgrid criterion specified. CONVERGE also includes an option for restricting y+ AMR when flow conditions are such that the subgrid scale near the walls trigger AMR. This feature was briefly investigated in this study, but

no results are presented. Another feature available in CONVERGE is grid scaling, which occurs when the base grid size is changed at a specified time during a simulation. It can greatly reduce runtimes by coarsening the grid during noncritical simulation times and can help capture critical flow phenomena by refining the grid at other times. In our study, the grid was coarsened during the first 20 ms to help get the flow field somewhat established before applying any mesh refinement.

3. Results and Discussion

3.1 RANS Analysis

RANS computations were performed with COMSOL to investigate their performance in predicting film-cooling effectiveness. Film cooling effectiveness is defined as

$$\eta = (T_\infty - T_{aw})/(T_\infty - T_c) \tag{1}$$

or

$$\eta_1 = (T_r - T_{aw})/(T_r - T_c), \tag{2}$$

where T_∞ is the inlet temperature, T_{aw} is the adiabatic wall temperature, T_c is the coolant temperature, and T_r is defined as the recovery temperature (adiabatic wall temperature) in a region that is not affected by the film cooling.

3.1.1 κ-ε Turbulence Model

COMSOL uses the finite element method to perform multiphysics simulations. The accuracy of the simulation, when using the finite element method, is linked to the size of the mesh. As the mesh size decreases, the solution approaches the exact solution for the equations being solved. But sometimes the computational resources available may dictate how small a mesh can be. The purpose of the simulation might also influence what size mesh to use. If the purpose is to investigate trends that would help guide a set of experiments, the solution might not need to be very accurate, and mesh size required might be within the computational capabilities at hand.

A series of computations were performed to investigate the smallest mesh size that could be used for this study with the computational resources available: a MacBook Pro laptop with 16 GB of memory running on four cores. The RANS computations were carried out using the κ-ε turbulence model. It uses wall functions and has a good convergence rate and relatively low memory requirements. Three mesh sizes were created using the automatic mesh-generation feature in COMSOL. The automatic mesh-generation feature takes into consideration the physics of the

problem being solved. The first mesh created was what COMSOL calls “coarse”. It had 249,534 elements and consisted of a combination of tetrahedrons, pyramids, prisms, and quad elements. The normal mesh consisted of 834,115 elements, and the fine mesh had 2,416,340 elements distributed among the shapes mentioned. A cross-section view of the three meshes is shown in Fig. 3. It clearly can be seen that the software adds significantly more elements at the plenum inlet, where the flow enters the cooling holes and where the air coming out of the cooling holes mixes with the freestream air flow.

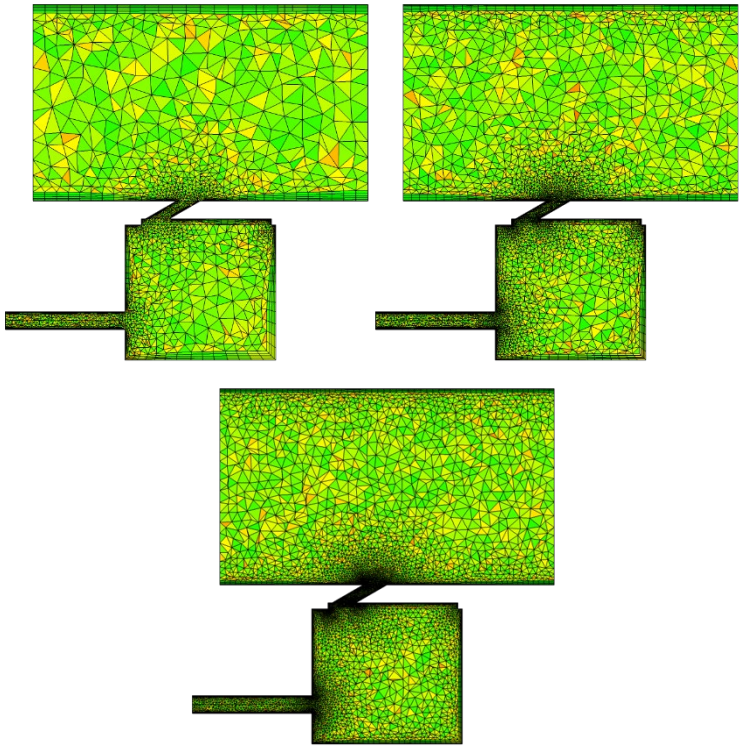

Fig. 3 Cross-section view of the meshes generated for the κ-ε turbulence model: (top left) coarse, (top right) normal, and (bottom) fine

It took less than 1 h to run the coarse mesh for both BRs. The normal mesh for the BR of 0.5 took about 50 min to complete the simulation and about 1 h and 26 min for the 1.0 BR case. When running the fine grid for both BR cases, COMSOL could not reach a converged solution. After consulting with COMSOL technical support, it was suggested that it was most likely due to an out-of-memory issue. Their suggestion was to use the one-way coupled, non-isothermal flow study available within COMSOL. Running the one-way coupled case took about 4 h to complete. The results were then used as the initial values for the fully coupled fine-mesh solution. It took less than 2 h to complete the fine-mesh computations for both BR cases.

Figure 4 shows the qualitative effect of mesh size on the computational results for the two blowing ratios studied, 0.5, and 1.0. The results presented are for the smooth plate only and are in the columns that have only two charts and plotted two ways. The top figure is calculated using Eq. 1, and the bottom figure is calculated using Eq. 2. T_∞ is the tunnel inlet temperature and T_r, the recovery temperature, is taken from the IR measurements at a location four diameters upstream of the holes. The computational results were calculated using Eq. 1. Qualitatively, the figure shows that as the mesh increases in refinement from coarse to fine, the computational results better match the experimental data. Since the accuracy of finite element method is directly related to mesh size, it is expected that the finer the mesh, the closer the results are to the experiments. Note that the initial computations did not include any heat transfer from the plenum to the plate. In these simulations, only the flow passages were modeled.

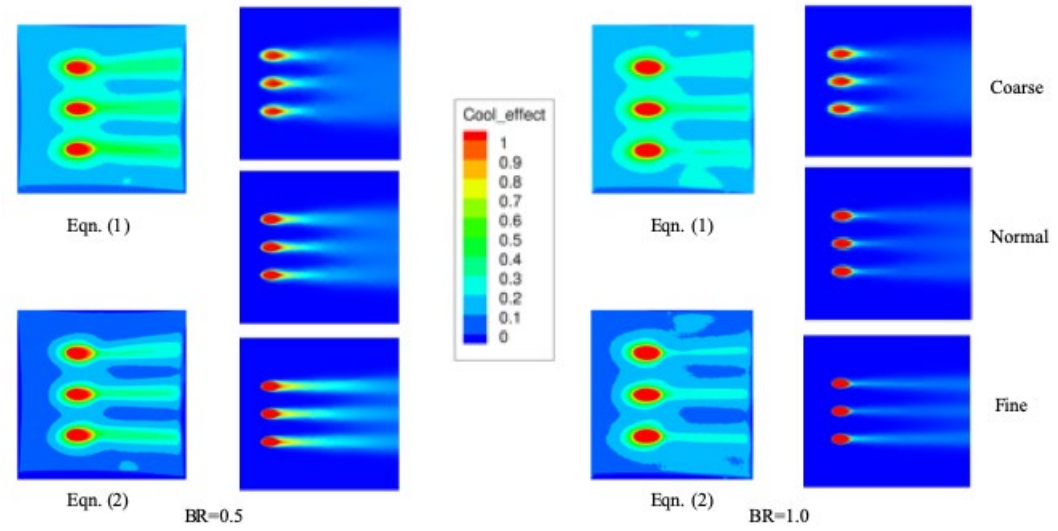

Fig. 4 Cooling effectiveness comparison of (left column) the experimental data and (right column) RANS COMSOL results with the k-e turbulence model. RANS results calculated using Eq. 1.

In Fig. 5, the cooling effectiveness at y = 0, the middle of the center cooling hole, is plotted as a function of the axial distance. The cooling effectiveness was calculated with Eq. 1. As shown in the figure, at BR = 0.5 the fine mesh does a fairly good job predicting the cooling effectiveness. The results for BR = 1.0 show that COMSOL is able to predict the profile of the cooling effectiveness experimental data closer than for the BR = 0.5 case but underpredicts the cooling effectiveness value. This is most likely the result of not including heat transfer in the initial computations. Heat transfer from the plenum below most likely will increase the surface temperature, and a higher surface temperature will result in a higher cooling-effectiveness value.

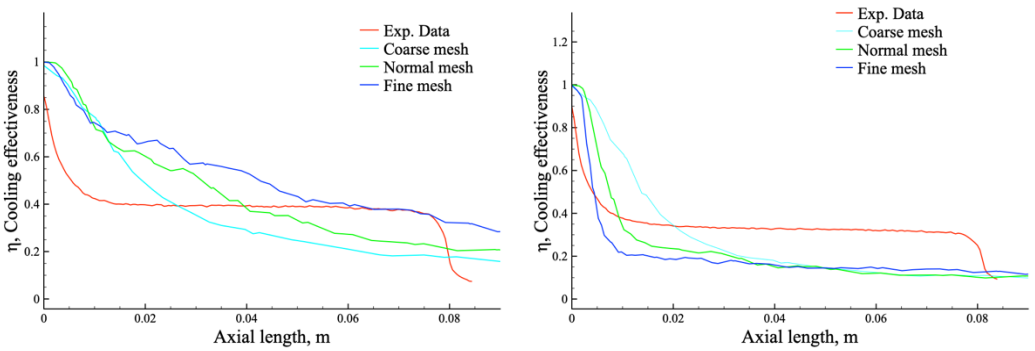

Fig. 5 Comparison of experimental data and cooling effectiveness computed with the COMSOL κ-ε turbulence model at y = 0 for (left) BR 0.5 and (right) BR 1.0

3.1.2 SST Turbulence Model

As noted elsewhere, the κ-ε turbulence model was chosen for this study for its good convergence rate and wide use. Of all the other RANS turbulence models available within COMSOL, the SST turbulence model was chosen because it is robust and widely used. It is a two-equation eddy-viscosity turbulence model that combines the κ-ε model in the freestream and the κ-ω model near the walls. It was formulated to eliminate some of the weaknesses in the pure κ-ω and κ-ε models. The κ-ω model is used in the inner region of the boundary layer and switches to the κ-ε model in the free shear flow.

The results for the SST turbulence model are shown in Fig. 6. The experimental results are shown in the left column and the computational results in the right column for each BR shown. The top figure in the experimental results column was generated using Eq. 1, and the bottom figure was generated using Eq. 2. Again, as expected for finite element methods, the finer the mesh, the closer the results are to the exact solution or the experimental data in this case. This particular case presented some challenges getting a converged solution. The coarse mesh had no issues converging, but the normal mesh did not converge. The one-way-coupled nonisothermal flow study available within COMSOL used to compute the κ-ε turbulence model fine-mesh results was attempted, but with no success. We next used the adaptive mesh-refinement feature also available in COMSOL. The default refinement method, known as mesh initialization, was used. It refines the mesh in areas where smaller elements are needed based on the physics and can also coarsen the mesh where a fine mesh is not needed based on a global metric. In this case the L2 norm of error squared was used as the refinement metric. The default is to do two levels of refinement. The mesh refinement was started from the coarse mesh solution. COMSOL refined the mesh once but encountered an error when generating the second mesh during the second level of refinement. A cross-section view of the coarse and refined meshes is shown in Fig. 6. The coarse mesh had

325,730 elements, and the refined mesh had 753,801. Note that the coarse mesh generated by COMSOL for the SST turbulence model is larger than the one generated for the κ-ε model. The SST model is considered a low-Reynolds-number model, but the κ-ε model is not. Low-Reynolds-number models, in general, require higher mesh resolutions, which COMSOL accounts for in its mesh-generation routines. Another difference between the adapted mesh and physics-based mesh is that instead of just reducing the mesh size globally, as shown in Fig. 3, the adaptation process increased the mesh resolution downstream of the cooling hole exit (i.e., following the jet trajectory).

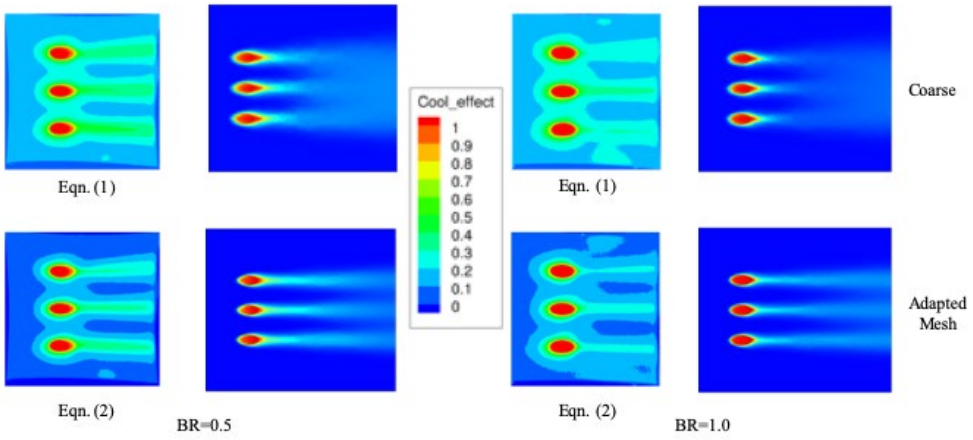

Fig. 6 Cooling effectiveness comparison of the (left column) experimental data and (right column) RANS COMSOL results with the SST turbulence model. RANS results calculated using Eq. 1.

As shown in Fig. 7, both meshes show fairly good agreement with the experimental data, as far as trends are concerned. The results shown in Fig. 8 confirm this observation. Both the coarse and adapted meshes capture the cooling effectiveness trend fairly well, but the adapted mesh follows the trend much closer for both BRs.

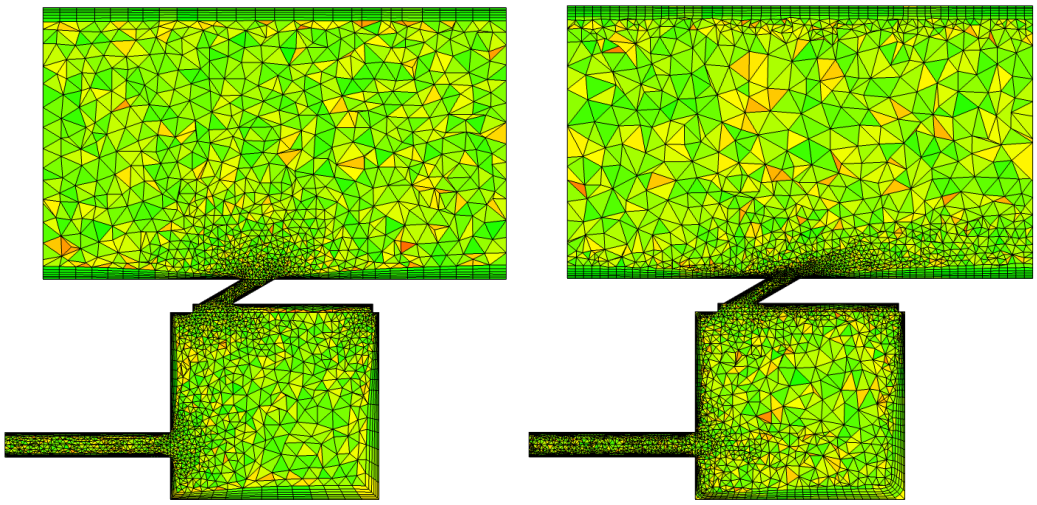

Fig. 7 Cross-section view of the meshes generated for the SST turbulence model: (left) coarse mesh and (right) adapted mesh

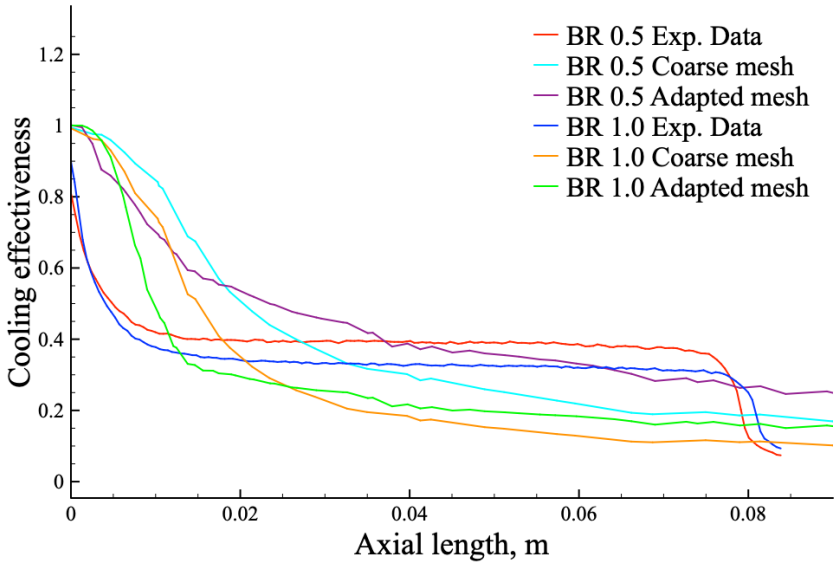

Fig. 8 Mesh comparison of computed cooling effectiveness vs. experimental data for the COMSOL SST turbulence model

A close comparison of the κ-ε model and the SST model results for the normal and adapted meshes, respectively, which are close in the number of total elements, showed that the SST turbulence model with the adapted mesh compares better with the experimental results than the κ-ε turbulence model with the normal mesh, as shown in Fig. 9. This is the result of the application k-omega in the inner region of the boundary layer and the mesh refinement applied downstream of cooling hole exit.

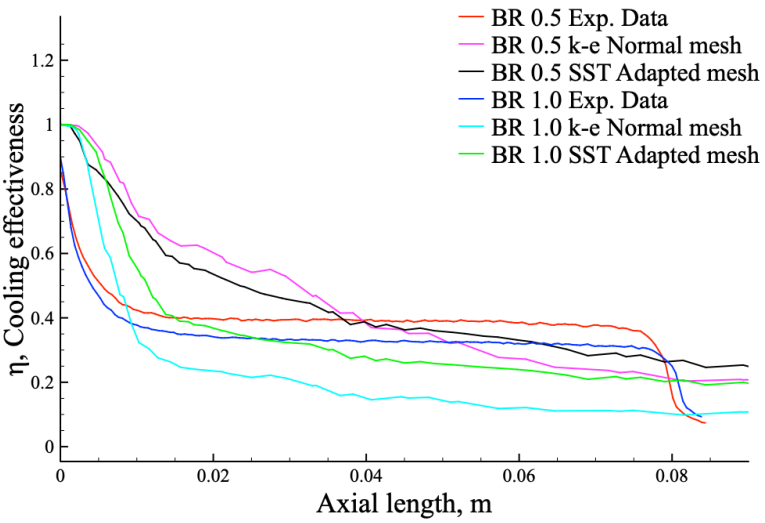

Fig. 9 Comparison between experimental data and cooling effectiveness computed with the COMSOL κ-ε and SST turbulence models at y = 0

3.2 LES Analysis

The LES simulations were carried out using the commercial CFD software CONVERGE running on the NASA Advanced Supercomputing Pleiades supercomputer. Pleiades is a distributed-memory SGI/HPE ICE cluster. A total of 220 cores were used for each simulation. Turbulence was modeled using the LES Dynamic Structure model available in CONVERGE. The model uses a tensor coefficient for the structure of the subgrid stresses and a subgrid kinetic energy for the magnitude of the stresses. The tensor coefficient is obtained directly from using the common "dynamic approach" using the Germano identity. The subgrid kinetic energy is obtained from a transport equation.[7] The meshes were generated using the automated mesh generation features available in the code. The process starts by selecting the base mesh size, for this study 2 mm. AMR was applied on the velocity to the whole computational domain but with different embedding levels in different regions. The freestream and the cooling holes were allowed two levels of embedding, while the plenum was allowed only one level. Embedding levels refer to the number of times the computational cell is allowed to split into smaller cells. There is also the option to add fixed embedded areas or volumes. It was applied to the surface of the cooling holes and the bottom of the tunnel. An embedded box was created extending 40 mm upstream of the trailing edge of the cooling hole and 120 mm downstream, 120 mm wide, and 90 mm tall. The embedded box can be seen in Fig. 10. The effect of AMR can be seen most notably in the cooling holes and downstream of the plenum inlet. The meshes consisted of about 6.3 million cells for the BR = 0.5 case and 6.1 million for BR = 1.0. Each computation took about 7 h of wall clock time to complete.

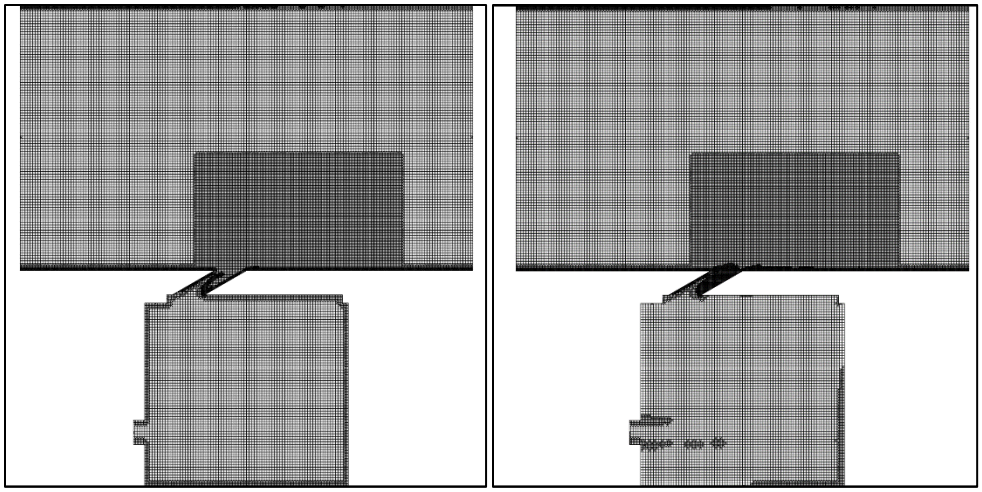

Fig. 10 Cross-section view of the meshes generated by CONVERGE: (left) BR = 0.5 and (right) BR = 1.0.

A qualitative comparison of the computational results is shown in Fig. 11 for both blowing ratios studied. The top figure for the computational results shows the cooling effectiveness computed at the last time step, and the figure below is a time-averaged solution over 30 ms. At BR = 0.5 it looks like CONVERGE overpredicts the cooling effectiveness. The CONVERGE results are closer to the experimental results at BR = 1.0. The results are plotted in Fig. 12. This confirms what was observed from Fig. 11. At BR = 0.5 the computations are overpredicted, and at BR=1.0 the computations are closer to the experimental data. Note again that these computations do not include heat transfer from the plenum to the tunnel bottom surface.

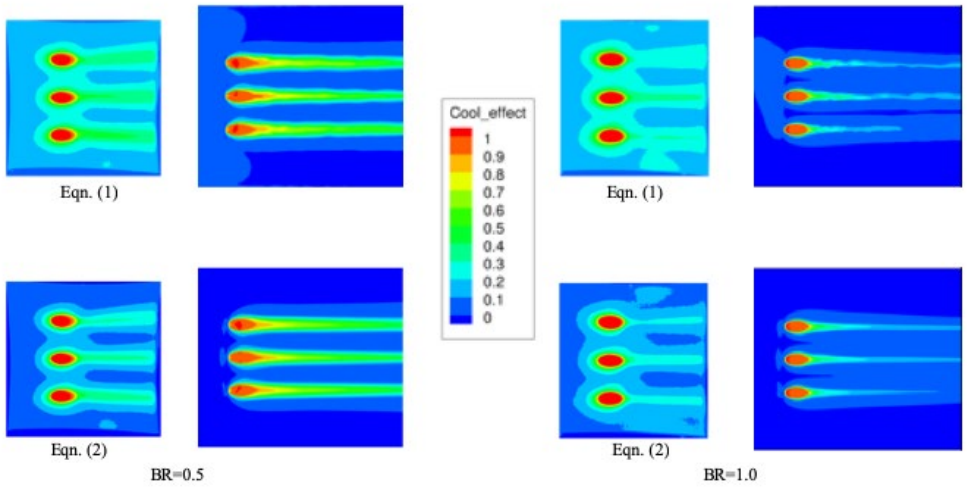

Fig. 11 Cooling effectiveness comparison of (left column) the experimental data and (right column) LES CONVERGE results. LES results calculated using Eq. 1

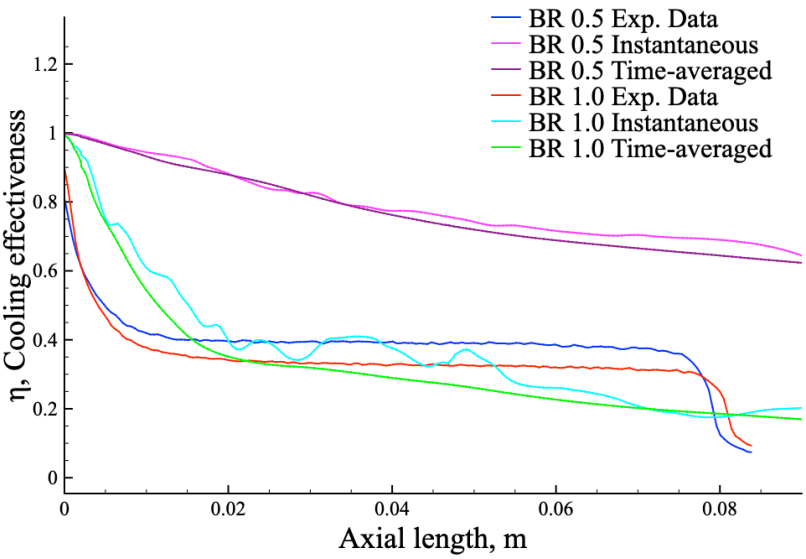

Fig. 12 Comparison of experimental data and CONVERGE LES cooling effectiveness results at y = 0

4. Summary and Conclusion

A computational study was carried out to investigate the potential of using commercially available CFD packages to evaluate potential film cooling hole configurations and quickly select those with the greater potential for experimental evaluation. This quick screen process would reduce the time and cost required to experimentally evaluate new and improved film cooling concepts.

The software packages COMSOL Multiphysics and CONVERGE were selected for this study. Both packages have automatic mesh-generation capabilities. COMSOL offers a time-saving step when trying to evaluate a potentially large number of design concepts. The computational results were compared with experimental data and showed that the meshes generated by both software packages were qualitatively and quantitatively in good agreement with the experimental data. Both provide substantive information to assess the potential of new proposed film cooling concepts in a timely manner, reducing experimental time and resources.

5. Future Work

New film cooling configurations have been conceived and will be evaluated to determine which ones will be selected for experimental evaluation. The addition of conjugate heat transfer will be investigated. The computations presented here were performed using a flat plate. The addition of computationally efficient ceramic matrix composite surface features will also be investigated.

6. References

1. Boyle RJ, Agricola LM, Parikh AH, Ameri AA, Nagpal VK. Shrouded CMC rotor blades for high pressure turbine applications. Proceedings of the ASME Turbo Expo 2018. Vol. 2B. doi: 10.1115/GT2018-76827.

2. Bogard D, Thole K. Gas turbine film cooling. J Prop Pow. 2006;22(2):249–270.

3. Bons JP, MacArthur CD, Rivir RB. The effect of high freestream turbulence on film cooling effectiveness. J Turbomach. 1996;118:814–825.

4. Shyam V, Thurman D, Poinsatte P, Ameri A, Eichele P, Knight J. Long hole film cooling dataset for CFD development. Part 1: infrared thermography and thermocouple surveys. Washington (DC): National Air and Space Administration; 2013 Nov. Report No: NASA/TM—2013-218086.

5. Shyam V, Thurman D, Poinsatte P. Ameri A, Culley D. Toward cooling uniformity: investigation of spiral, sweeping holes, and unconventional cooling paradigms. Washington (DC): National Aeronautics and Space Administration; 2018 Mar. Report No: NASA/TM—2018-219763.

6. Sgarzi O, Leboeuf F. Analysis of vortices in three-dimensional jets introduced in a cross-flow boundary layer. New York (NY): American Society of Mechanical Engineers; 1997. ASME Paper No.: 97-GT- 517.

7. Chumakov S, Rutland CJ. Dynamic structure models for scalar flux and dissipation in large eddy simulation. AIAA Journal. 2004;42(6):1132–1139.

List of Symbols, Abbreviations, and Acronyms

ABS	acrylonitrile butadiene styrene
AMR	adaptive mesh refinement
BR	blowing ratio
CFD	computational fluid dynamics
CMC	ceramic matrix composite
D	diameter of film cooling hole
GUI	graphical user interface
HPT	high-pressure turbine
IR	infrared
L	length of film cooling hole
L/D	length-to-diameter
LES	large eddy simulation
NASA	National Aeronautics and Space Administration
P	spacing between film cooling holes
PC	personal computer
P/D	pitch-to-diameter
RANS	Reynolds-averaged Navier–Stokes
SST	shear stress transport
T	temperature

Greek alphabet

ε	rate of turbulent kinetic energy dissipation
κ	turbulent kinetic energy
η	film cooling effectiveness
ω	specific rate of dissipation

Subscripts

aw	adiabatic wall

c	coolant
∞	freestream
r	freestream recovery

1 (PDF)	DEFENSE TECHNICAL INFORMATION CTR DTIC OCA
1 (PDF)	CCDC ARL FCDD RLD CL TECH LIB
1 (PDF)	CCDC ARL FCDD RLV P W BRENNAN